The International Archives of the Photogrammetry, Remote Sensing and Spatial Information Sciences, Volume XLVIII-5/W4-2025
Philippine Geomatics Symposium (PhilGEOS) 2025 "Enhancing Human Quality of Life through Geospatial Technologies",
24–25 November 2025, Quezon City, Philippines

Modeling the Contribution of Land Subsidence to Water Level Change in Former Boneng Mine Site Using Multi-Temporal InSAR

Katelyn Reese G. Dizon[1], Luis Carlos S. Mabaquiao[1], Rosalie B. Reyes[1]

[1]Department of Geodetic Engineering, University of the Philippines, Diliman, Quezon City, Philippines –
kgdizon@alumni.up.edu.ph, (lsmabaquiao, rbreyes3)@up.edu.ph

Keywords: InSAR, Land Subsidence, LiCSBAS2, Water Level Changes, Generalized Additive Model

Abstract

There are 27 recorded abandoned mines within the Philippines. Unfortunately, there is insufficient data regarding the history, features, and current impact of abandoned mines on the locale. This study proposes the usage of remote sensing techniques as an alternative for quantifying and modeling the occurrence of land subsidence near mine pit lakes using the former Boneng mine (currently Lubo Lake) as the primary study area. Ground deformation values (averaged 3.3 mm/yr vertical velocity for the entire site) from 2015 to 2021 were derived from Sentinel-1 images. Lake water level changes (averaged at -0.665 m/yr for summer seasons and 1.613 m/yr for rainy seasons) were estimated through Normalized Difference Water Index (NDWI) calculations, vectorization, and geometric transformations. The contribution of land subsidence to the lake water level, along with other geologic and climate features, and predicted changes were modeled using a Generalized Additive Model (GAM). Land subsidence was found to affect the water level changes of the lake. However, its significance and overall predicted effect could not be generalized into a pattern or trend by the GAM.

1. Introduction

1.1 Background

Abandoned mines are mines that operated under a mining lease or mineral agreement contract but halted operations without a proper decommission process (Samaniego et al., 2020). Mine pit lakes develop in the aftermath of an open-pit mining closure (State of Nevada Department of Conservation & Natural Resources, n.d.). These function similarly to hydrological sinks and may pose harmful environmental effects due to limited outflow, varied water quality, and enlarged water volume (Castro & Moore, 2000). Furthermore, land subsidence begins to occur as a water body continues to increase its water volume (Wahr et al., 2001).

There are 27 recorded abandoned mines in the Philippines (Aggangan, et al., 2019). Among that list is the Western Minolco Mining Company that operated the Boneng Mine site— now referred to as Lubo Lake (Raymundo, 2017). Many abandoned mine pit lakes throughout the Philippines lack fundamental data regarding their history, features, and current impact on the local area. The information gap causes additional hurdles against the effective execution of pit lake management projects and strategies. Furthermore, in-situ monitoring systems and regular site visitations are an expensive venture that many local government units cannot afford.

1.2 Objectives

The goal of the study is to analyze the contribution of land subsidence to water level changes in the former Boneng Mine site. The study also aims to derive land subsidence and water level data only using remote sensing techniques, use those results to model the relationship between the two, while accounting for climatological effects, and give key insights on how future land subsidence occurrence may affect water level changes.

1.3 Significance

According to an online report published by the Mines and Geosciences Bureau (MGB), regular visitations to abandoned mines are held to assess the condition of structures in the area. These areas have been forsaken since the operation closure, but have been resettled and repurposed by locals. For the case of the former Boneng Mine, the site is still officially closed to public visitations (RPN Social, 2022). However, in reality, online posts advertise it as a tourist spot and say it is used to raise tilapia (The Cordilleran Sun, 2018).

Land subsidence occurs as a water body increases its water levels (Wahr et al., 2001). Land subsidence can lead to infrastructure damage, ecosystem disruption, and permanent groundwater storage changes (Ndahangwapo, et al., 2024). However, only select areas are actively monitored for land subsidence due to limited budget and personnel (Chang, et al., 2007).

The processes employed in the study may be used by the MGB and other mining-related companies or organizations as an alternative method for obtaining information on the condition and hazards of mine pit lakes. Usage of remote sensing techniques can cut down mine assessment costs and assist in mine rehabilitation projects. Moreover, the study will help inform and prepare locals for possible ground deformation occurrences.

1.4 Scope and Limitations

The study is only concerned with the vertical land motion induced in the former Boneng Mine site. The time frame considered only data from 2014 to 2021. However, older supplemental data, such as the oldest IFSAR data and the geologic map of the mine pit, were also considered.

Implementation of this study was officially endorsed by the MGB - Central Office. However, even with the official endorsement, the governing LGU for the study area refused site access for ground validation. Upon consultation with the Officer in Charge for the Mines and Geosciences Bureau - Cordillera Administrative Region (MGB-CAR) Mine Safety, Environment, and Social Development Division, it was recommended to cease site access for safety reasons. These developments caused limitations to the data validations. For water levels, all value derivations were recognized as merely proxy values.

2. Materials and Methods

2.1 Study Area

The former Boneng Mine Site (currently Lubo Lake) is located in Kibungan, Benguet of the Cordillera Administrative Region with the geographical coordinates of 16° 38' 16" North, 120° 40' 36" East. The extent of the study area is a rectangular boundary with an approximate length of 5.33 km, a width of 3.32 km, and an area of 17.74 km. The selection of the former Boneng Mine site as the study area was based on the recommendation of MGB-CAR. The selection was also influenced by the lack of concrete information regarding the past and present condition of mine pit lakes for assessment of potential hazards and monitoring (Brillo, 2022).

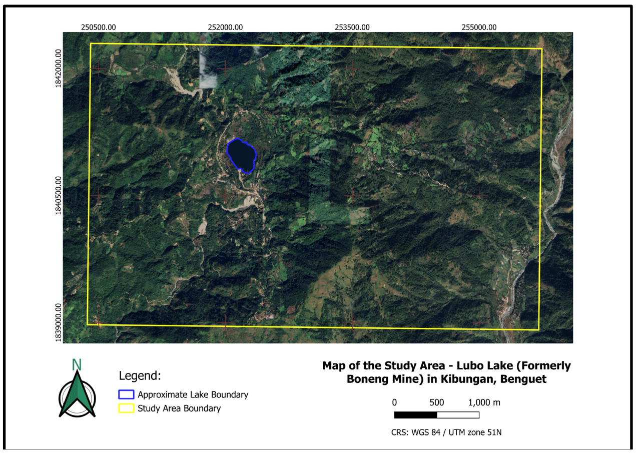

Figure 1. Map of the Study Area

2. 2 Data Requirements

The LiCSBAS2 software was optimized to use LiCSAR (Looking Continents from Space Automated Radar) products for its Interferometric Synthetic Aperture Radar (InSAR) time-series processing. LiCSAR products were derived from Sentinel-1 images and are publicly available from the COMET-LiCS web portal. Products covering the study area have a frame ID of 142A_07411_111313 with an ascending orbit direction. All available products from October 10, 2014 to December 12, 2021 were collected.

Images captured by Sentinel-1 and Sentinel-2 were obtained for the water level estimation. Requirements for the images were an acquisition mode of Interferometric Wide Swath (IW) of 10 m x 10 m resolution, polarization of VV+VH, and a cloud coverage of 30% or below. Satellite images from March 2014 to October 2021 were used to match the time interval of the ground deformation results from LiCSBAS2. Specifically, two images per year were considered for water level estimation. These were the annual March and October images to represent the rainy and dry seasons of the Philippines respectively.
Other supplemental datasets used included a 2013 Interferometric Synthetic Aperture Radar - Digital Elevation Model (IFSAR - DEM) of the study area from National Mapping and Resource Information Authority. Historical climate data was originally requested from the Philippine Atmospheric, Geophysical and Astronomical Services Administration, but no response was received. As an alternative, climate data was obtained from the international archive for global weather and climate data. A geologic map of the Atok Quadrangle of Benguet dated 1996 was provided by the Geology Division of MGB-CAR.

2.3 Methodology

The general methodology is outlined in Figure 2 below.

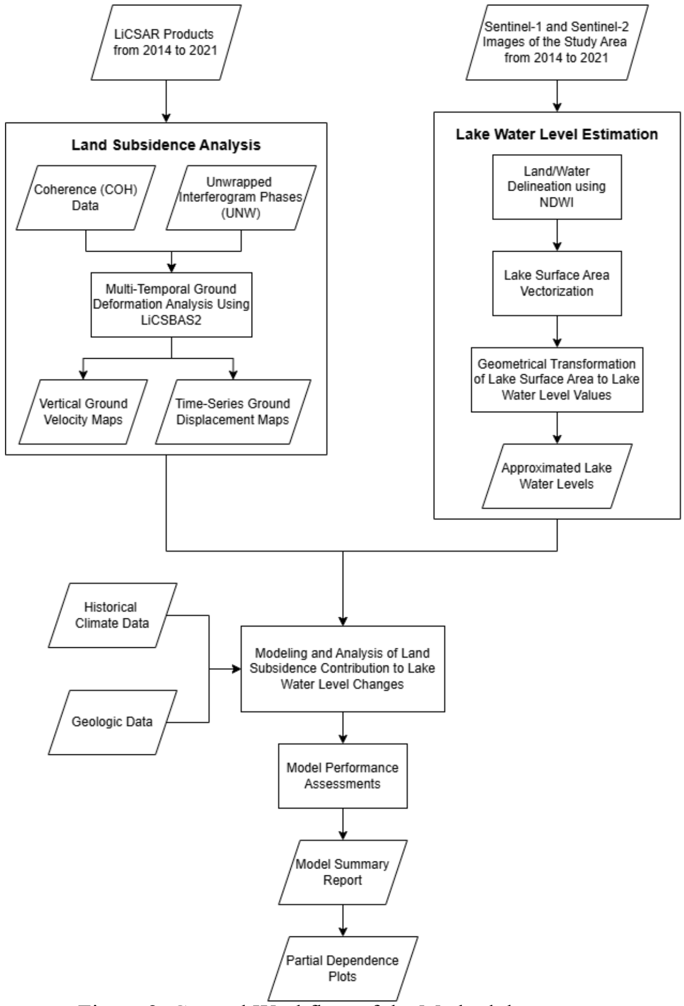

Figure 2. General Workflow of the Methodology

For the Land Subsidence Analysis, multiple master-slave interferogram pairs were used rather than designating a single master for an entire image stack. Master-slave pairs were created by pairing images with the shortest temporal and spatial baselines. The image with the earlier acquisition date was designated as the master image. All interferogram pairs were combined according to the oldest acquisition date, then calculated using least squares to derive the time-series deformation per pixel.

For Lake Water Level Estimation, satellite images were selected based on satellite type, prioritising those from Sentinel-2, and study area visibility. Selected images underwent Normalized Difference Vegetation Indices (NDWI) calculation, lake surface area vectorization, and then geometric transformation to derive water level values.

Finally, for the Modeling and Analysis using Generalized Additive Model (GAM), outputs from the two prior sections were collated and combined with geologic and historical climate data. Lake water level changes were designated as the target variable, while other parameters were designated as features or independent variables. GAM used iterative machine learning methods to calculate the best-suited smoothing parameter (λ) and number of splines (n) for modeling the relationship between the target variable and all other features.

2.3.1 Land Subsidence Analysis: Small Baseline Subset (SBAS) was chosen as the primary InSAR technique for calculating the time-series ground deformation. Synthetic Aperture Radar (SAR) images with the shortest spatial and temporal baseline from each other were paired to create interferograms. These interferogram pairs were co-registered to ensure geometric consistency across the time-series network. The interferogram pairs were unwrapped separately, then "suitable points" or points with high coherence were identified in the network (Anjasmara, et al., 2020; Li, et al., 2022). SBAS was chosen for its ability to densify "suitable points" in rural areas and surfaces with little to no artificial structure. Given the nature of the study area, there was almost no infrastructure left over from when the mine was active. Some build-up from resettlement of locals was identified, but they remain few and far between. Most, if not all, of the "suitable points" would come from benches and dirt roads that remained from the mine's operation phase.

Each interferogram underwent a filtering process to remove COH (coherence) and UNW (unwrapped) datasets that did not meet the threshold value. The small baseline network of the UNW data was inverted to obtain the time-series and velocity using Least Squares. No weights were used during the inversion. The small baseline inversion allowed the software to identify stable reference points across the interferograms. Afterwards, the standard deviation of the vertical ground velocity was calculated using the bootstrap method and spatio-temporal consistency. An output quality check was performed to mask pixels with high noise indices from the time-series. Finally, a filtering and de-ramping process was performed to calculate the velocity of the time-series.

Two main outputs of the LiCSBAS2 software were (1) a geoTIFF file of the average cumulative vertical ground velocity per pixel across the time-series and (2) the exact ground displacement of pixels that passed the masking process (those deemed to have low noise indices) per interferogram acquisition date.

2.3.2 Lake Water Level Estimation: Each image underwent land/water delineation through NDWI computation. The indices were used to discriminate the lake from other land cover types (Quang et al., 2021). The surface area of the lake was vectorized and calculated using QGIS.

Due to the unavailability of a bathymetric map or updated digital elevation map, water levels could only be approximated by geometrically transforming the lake surface area into its corresponding water level value. A mathematical equation was derived by assuming that: (1) the lake is represented as a conical object, (2) the lake is assumed to be like a cone-shaped basin, and (3) the sides of the basin are sloped. These assumptions were based on the study area's former nature as an open-pit mine. The base equations used are the area of a cone and the trigonometric relationship of radius, height, and slope.

$$h = \sqrt{\frac{A}{\pi tan^2(\theta)}}, \tag{1}$$

where A = Lake surface area (m²)
h = Water level (m)
r = Slope

Slope value was derived through a generated slope map from the IFSAR image of the study area.

2.3.3 Modeling and Analysis Using Generalized Additive Model (GAM): Dataset inputs for the model were limited to results of the prior processes to adhere to the study's goal of a replicable and low-cost method for deriving information on abandoned mine pit lakes. However, the imposed dataset limitation negatively affected the model's predictive quality. GAM was deliberately chosen to address this trade-off between dataset limitation and predictive quality. GAM, as a parametric model, required a small amount of data while remaining stable across its computational process (Bzdok & Yeo, 2017). Controllability of smoothing parameters to avoid overfitting and underfitting was another advantage of GAM (Carnegie Mellon University, 2014). In addition, the probable relationship between features and the target variable was too uncertain to make initial assumptions on whether the relationship is linear or nonlinear. Usage of GAM allowed for flexibility for both relationships. Linear relationships were excluded from smoothing parameter calculations, while nonlinear relationships underwent further iterative computations for the "best" parameter combination.

The two dataset inputs for the model were narrowed down to the GeoTIFF from LiCSBAS2 and the CSV of key pixels. The geoTIFF file of the averaged cumulative ground velocity values was used as it is. The coordinates of the key pixels were listed in a CSV file. These pixels were discriminated as ground or water pixels by identifying whether they were within or crossed the vectorized lake surface area. Then each pixel was attributed with quantified values for ground deformation, climate data, and geology type. Precipitation rates for both seasons were readily available from the historical climate data. Evaporation rates were calculated using the Dalton-type equation (Wei et al., 2021) and the modified Magnus equation for approximating vapor pressure (Alduchov & Eskridge, 1996). The geologic map from MGB-CAR stated all present rock types, but not the composition percentage per rock type. The entire study area was generalized into one rock type. As such, rock type was not included in the model.

The GAM script was implemented in Python. The model separately processed the data for summer and rainy seasons to reduce model training complexity and allow for better feature relationship analysis. The script read the CSV and filtered for the seasonal data to be used in that run (rainy or summer). The GeoTIFF file was opened to extract the averaged cumulative vertical ground velocity per pixel. Filtered data from the CSV were merged with extracted values from the geoTIFF into a dataframe. The water level values were designated as the target variable (y) while all other features were designated as features or independent variables (x).

The model was trained using the training set, and then the predicted values were compared with the testing set to measure model accuracy. The generally accepted validation method for machine learning based models without ground truth data is the 70-30 or 80-20 data split (Sekkeravani, et al., 2021; Fengkai, et al., 2022). The 80% training set and 20% testing set split was chosen due to the low number of data points from the CSV input file. Designating a higher percentage for the training data provided the model with more samples in identifying patterns across data points. A set of spline values and a regularization strength (λ) range was predefined for each term. Then, the best-suited λ for each spline value was iteratively calculated using hyperparameter tuning. The spline and λ value combination with the lowest test RMSE was chosen as the best predictive model parameters.

Model performance assessments were performed by calculating the RMSE (Root Mean Square Error), R², deviance explained, and 5-Fold Cross-Validation. Additional flags for model overfitting or underfitting were included. Partial dependence plots were produced to visualize the relationship of the target variable with other features.

3. Results and Discussion

3.1 LiCSBAS2-Derived Ground Deformation Values

602 interferograms were obtained during the LiCSBAS2 preparation phase. The interferogram underwent three quality filtering phases to remove those that failed to meet threshold values and/or had high noise indices. Only 128 out of 602 interferograms were used.

The time-series for cumulative ground displacement (mm) and vertical ground velocity values (mm/yr) from 2015 to 2021 was displayed upon completion of the LiCSBAS2 process, as shown in Figure 3. Both the time-series and vertical velocity are given in two spatial outputs: all pixels covering the study area boundary and only pixels that passed all filtering and masking processes. Spatial resolution for the generated outputs is 30 m x 30 m.

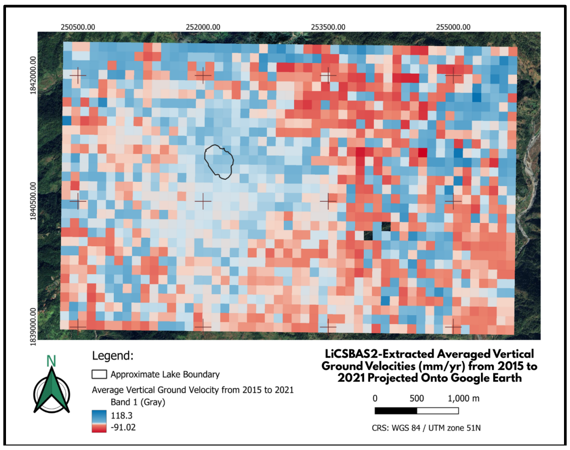

Figure 3. Map of the LiCSBAS2-Extracted Averaged Cumulative Vertical Ground Velocity (mm/yr)

The spatial resolution was relatively low, given the small size of the study area, and was expected to negatively affect the accuracy of the results. High coherence values were found in the pixels that fully corresponded to the lake; these were considered erroneous since SAR signals cannot penetrate through water. The lake water pixels were masked out to address this concern. Only pixels on the boundary of the lake and beyond those were considered for the succeeding processes.

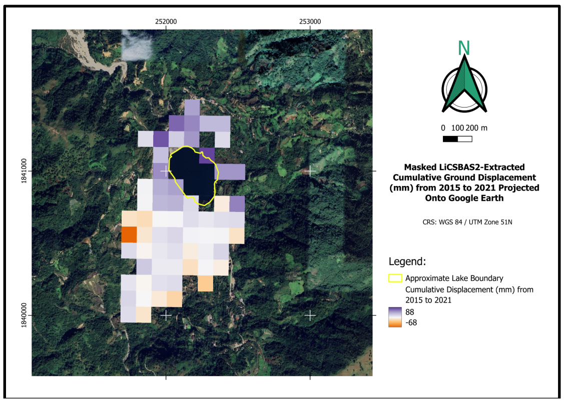

Figure 4. Map of the Masked LiCSBAS2-Extracted Cumulative Ground Displacement (mm)

71 key pixels remained after filtering low coherence and/or erroneous pixels. The cumulative displacement of the key pixels was plotted to visualize their movement throughout the time-series.

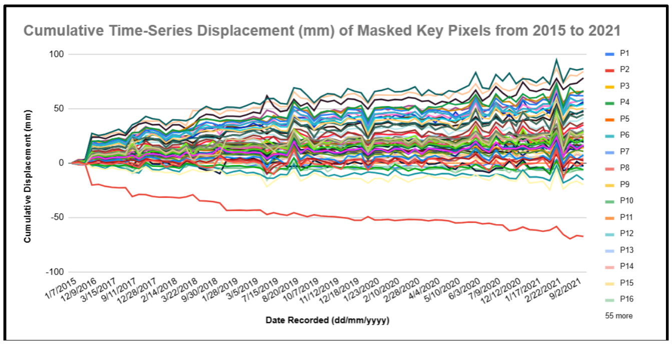

Figure 5. Plot of the Cumulative Time-Series Displacement (mm) of Masked Key Pixels from 2015 to 2021

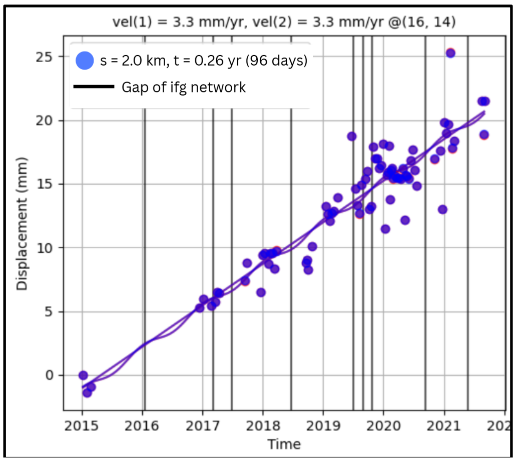

Figure 6. Plot of the LiCSBAS2 Generated Masked Time-Series Vertical Ground Displacement from 2015 to 2021 (mm)

Primary visual inspection. Figures 4, 5, and 6 show that the ground surrounding the lake was experiencing uplift while the area outside was experiencing subsidence. The vertical velocity is relatively small (3.3 mm/yr), indicating that the ground remains fairly stable. However, the occurrence of uplift and ground subsidence within the same area may indicate ground instability due to the occurrence of sediment deposition towards the lake. Annual vertical velocity was summarized in Table 1.

Year	Average Displacement (mm)
2015	0.406
2016	8.119
2017	9.935
2018	13.167
2019	18.178
2020	21.024
2021	24.802

Table 1. Average Ground Displacement of the former Boneng Mine (Lubo Lake) Area per Year

Ground displacement and vertical ground velocity values cannot be validated with ground truth data. However, according to a study that compared LiCSBAS2 LOS (Line of Sight) velocity with GNSS LOS velocity measurements across the country. Three areas with lower correlations due to sparse data and small intervals have an ascending track LOS velocity difference of 4.1 to -17.4 mm/yr (Sulapas et al., 2024). The LiCSBAS2-derived ground deformation values for this study also utilized the ascending track, hence were assumed to have a similar millimeter-level accuracy. Note that these locations were recorded in metropolitan areas and may not be fully compatible with the study area. However, if the dataset quantity and time-series interval were considered instead, the comparisons become a better alternative validation.

3.2 Derived Lake Water Level Values

NDWI values for the images were calculated and were set to the same range to ensure consistency across all raster images. Lake water pixels were identified, and the lake surface area was manually vectorized as shown in Figures 7 and 8.

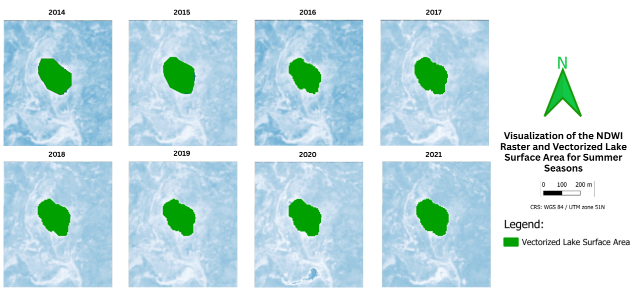

Figure 7. Visualization of the NDWI Raster and Vector Lake Surface Area for Summer Season from 2014 to 2021

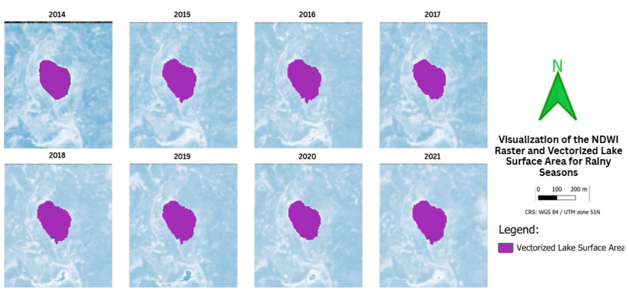

Figure 8. Visualization of the NDWI Raster and Vector Lake Surface Area for Rainy Season from 2014 to 2021

The vector surface area (m^2) was calculated, then geometrically transformed into water levels using the derived equation.

Year	Summer Season	Rainy Season
2014	333.004	341.468
2015	333.811	353.049
2016	315.594	355.110
2017	334.254	343.575
2018	327.482	347.327
2019	324.376	347.698
2020	328.014	335.644

Table 2. Calculated Lake Water Levels (m)

Water levels for the rainy season were higher, but the difference in water levels is relatively small except for those during 2016. The lake water level changes from the previous year were calculated by setting the water level for 2014 as the baseline.

3.3 Generalized Additive Model

The GeoTIFF from LiCSBAS2 and the CSV file of key pixels and their features were input into the model. 427 data points (71 key pixels combined with 6 years of quantitative values) were inputted and used for the 80-20 training and test data split. Summer and Rainy season datasets were modeled separately. Model performance metrics are unitless and compared by assessing the difference between train and test values. High differences indicate overfitting or underfitting.

3.3.1 Model Performance Assessment: No flags were raised for the summer model. The small difference between RMSE values indicates fairly good performance on unseen data. The summer model could predict future water level changes with an approximate 4.20 ± 0.28 prediction error. The model performs slightly better on the training data, but the small gap in train and test RMSE values indicates that the model generalizes patterns in the relationship between features fairly well. The summer model was able to explain 16% of the training data variance and 12% of the unseen data variance.

Metric	Summer Model	Rainy Model
Cross-Validation RMSE (5-fold)	4.20 ± 0.28	3.10 ± 0.37
Train RMSE	4.02	3.07
Test RMSE	4.31	2.47
Train R^2	0.160	0.241
Test R^2	0.120	0.100
Deviance Explained (Test)	16.0%	24.1%
Flag for Underfitting or Overfitting	No Flags Raised	Potential Overfitting

Table 3. GAM Performance Assessments Summary

Flags for overfitting were raised for the rainy model. The rainy model memorized the training set and failed to generalize to new data. There was a 0.6 difference between the RMSE values, indicating that the model performs better in the training data than on unseen data. The rainy model has an approximate 3.10 ± 0.37 prediction error when given a new dataset. The rainy model has a higher deviance explained value at 26.7% but performed worse compared to the summer model.

Overfitting in the rainy model was likely due to higher data variability, small sample size, limited temporal frequency, and coarse spatial resolution. It could also be linked to other unmeasured hydrological factors caused by intensified rainfall, such as surface runoff, water infiltration, and percolation. The said factors had little impact during summer seasons, but their effects were amplified during rainy seasons. This caused complex changes for rainy seasons, making it difficult for the model to recognize a general pattern and calculate predictions.

3.3.2 GAM Summary Report: Effective Degrees of Freedom (EDoF) quantified the "flexibility" or how much a feature can deviate from the training data. Yearly Ground Displacement was given the highest EDoF value, followed by Average Cumulative Ground Velocity for 2015 to 2020, then the Evaporation Rate after hyperparameter tuning. Both models gave a 0 EDoF for Precipitation Rate, meaning there is a linear relationship between Water Level changes and the Precipitation Rate.

Feature (Independent Variable)	Summer Model	Rainy Model
Average Yearly Ground Displacement (short-term ground deformation)	10.3	7.1
Average Cumulative Ground Velocity for 2015 to 2020 (long-term ground deformation)	6.4	4.2
Evaporation Rate	4.1	3.8
Precipitation Rate	0	0

Table 4. EDoF of each Feature Correlated with Water Level

GAM p-values were artificially low since the model estimates smoothing parameters for each feature. P-values were only used as a secondary metric. The summer model found that both long-term and short-term ground deformation had the greatest impact on water level changes, while evaporation rate was deemed to be insignificant. The rainy model found both ground deformation features to be insignificant and that climate factors had the greatest impact on water level changes.

Feature (Independent Variable)	Summer Model	Rainy Model
Average Yearly Ground Displacement (short-term ground deformation)	9.61×10^{-1}	8.24×10^{-13}
Average Cumulative Ground Velocity for 2015 to 2020 (long-term ground deformation)	9.99×10^{-1}	2.14×10^{-31}
Evaporation Rate	5.69×10^{-10}	3.28×10^{-6}
Precipitation Rate	6.69×10^{-2}	2.37×10^{-1}

Table 5. P-value of each Feature Correlated with Water Level

3.3.3 Partial Dependence Plots (PDPs): The resulting PDPs could not be taken as a direct representative of the relationship between water level changes and each feature due to the low deviance explained values across both models. However, the said values were good enough that the PDPs were still serviceable for drawing generalized trends or patterns on the variable relationships.

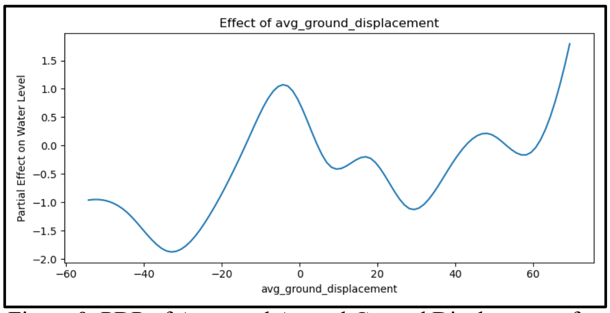

Figure 9. PDP of Averaged Annual Ground Displacement for Summer Seasons

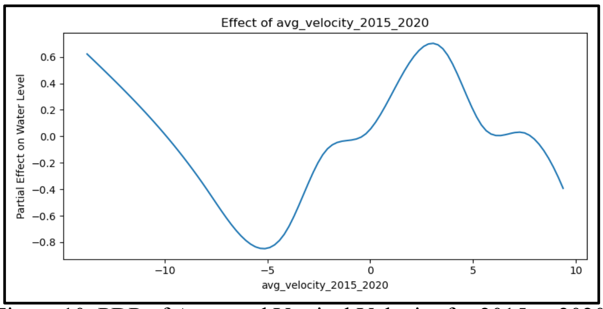

Figure 10. PDP of Averaged Vertical Velocity for 2015 to 2020 for Summer Seasons

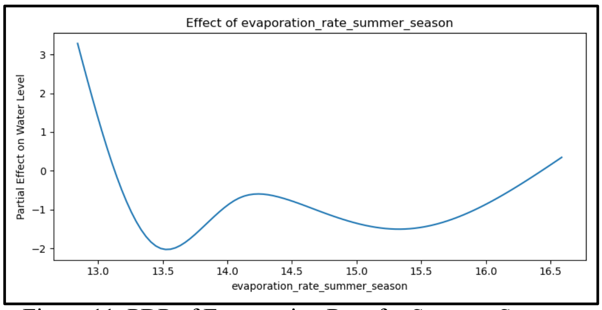

Figure 11. PDP of Evaporation Rate for Summer Seasons

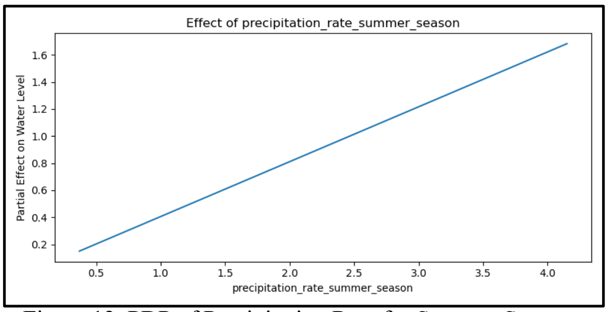

Figure 12. PDP of Precipitation Rate for Summer Seasons

For the summer model, short-term ground deformation showed impacts on water level changes. Some fluctuations in water level changes were present, but water levels were generally predicted to increase as the ground uplifts. The relationship with the water level became more complex through time. Uplift was predicted to initially cause an increase in water levels until the highest water level was reached. Afterwards, long-term uplift eventually resulted in a decline in water level. In the context of this model, long-term uplift seemed to be taken to an extreme— inclusion of long-term geologic transformation wherein the pit lake continued to uplift until it formed a hill.

For the climate features, the evaporation rate was predicted to have a somewhat logarithmic relationship with water level changes. Meanwhile, precipitation rate was predicted to have a direct linear relationship with water levels.

While a relationship was identified in the summer model, a denser dataset was required to fully encapsulate whether land subsidence has a significant contribution to water level changes. P-values were too low to be used as the main quantitative measurements for significance, and the PDPs themselves are not enough to provide quantitative measures for the relationship significance.

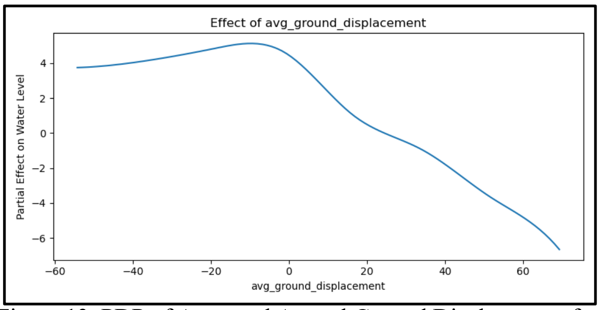

Figure 13. PDP of Averaged Annual Ground Displacement for Rainy Seasons

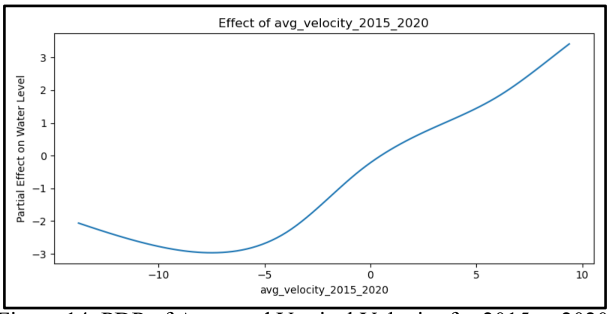

Figure 14. PDP of Averaged Vertical Velocity for 2015 to 2020 for Rainy Seasons

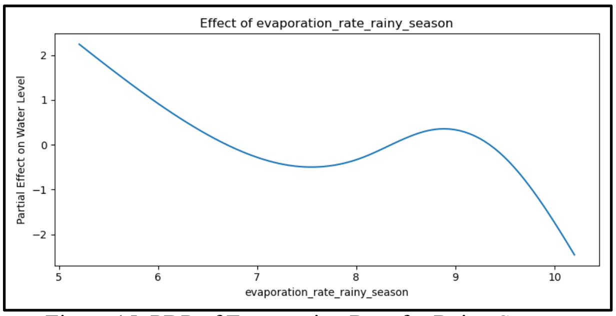

Figure 15. PDP of Evaporation Rate for Rainy Season

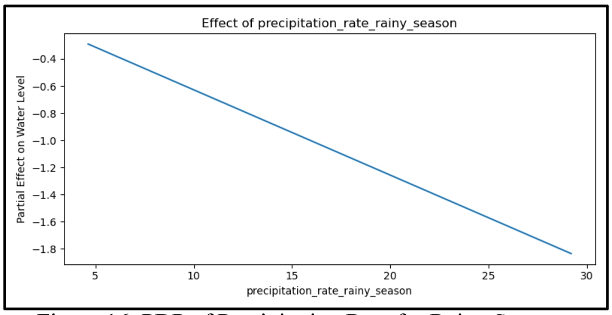

Figure 16. PDP of Precipitation Rate for Rainy Seasons

For the rainy model, ground deformation features (short-term and long-term) were predicted to have opposite effects. Short-term ground deformation was predicted to decrease water levels as the ground uplifts, while long-term ground deformation was predicted to cause high water levels as the ground continued to uplift. Since the rainy model was flagged to be overfitted, these opposing predictions could have been due to high variability in both ground deformation values. The dataset variability was too complex for the GAM algorithm and required a larger dataset to remedy overfitting issues. Moreover, the low p-values of the features indicated that they were not significant enough to have any obvious effect on water level changes. As such, no generalized pattern for the effect of ground deformation features on water level change could be made for the rainy model.

For climate features, the water level was predicted to generally decrease as the evaporation rate increases. Precipitation rate was still predicted to have a linear relationship with water level.

4. Conclusion

Ground deformation occurrence from 2015 to 2021 in the former Boneng Mine (Lubo Lake) was calculated using the SBAS-InSAR technique through the LiCSBAS2 software. Time-series for cumulative ground displacement (mm) and vertical ground velocity (mm/yr) maps from 2015 to 2021 were produced. Both subsidence and uplift were observed to occur in the study area. Specifically, the lake and its surrounding ground were experiencing uplift while the area past the lake was experiencing subsidence. This showed the occurrence of sediment deposition towards the lake. However, the time-series vertical ground velocity values remained relatively small from 2015 to 2021 (3.3 mm/yr), indicating that the ground remains fairly stable over time.

Water levels of the lake for summer and rainy seasons from 2015 to 2021 were estimated using a combination of land/water delineation using NDWI, lake surface area vectorization, and geometric transformation.

The relationship between water level changes and ground deformation, along with climate data, was modeled using GAM. It was determined that both long-term and short-term ground deformation had an impact on water level changes of the mine pit lake, but its significance could not be quantitatively measured with the current available dataset. Moreover, the predicted effects of ground deformation differed according to the season modeled. The overall predicted effect could not be generalized into a pattern or trend. The model deemed this relationship in the rainy seasons to be too complex, resulting in overfitting issues for the rainy season dataset. This could be remedied by providing more hydrological and climatological data for rainy seasons.

The techniques utilized to derive and calculate both ground deformation occurrence and water level changes could not be verified with ground truth data. Hence, all quantified values were only recognized as mere approximations. Nevertheless, the techniques utilized were proven to be a successful method for extracting ground deformation data and water level estimates for unmonitored abandoned mine pit lakes. The processes were replicable to other abandoned mine pit lakes, provided that the area is visible in satellite images. The generated results could be used for initial assessments on the site's general conditions, but it is recommended to use actual ground measurements to gain better insights. Water level estimations could be validated by measuring site water levels using a water level staff or other similar instruments. The addition of a new drone-captured DEM and better climate data from PAG-ASA would also increase the accuracy of the results. Moreover, additional verification using GNSS-station data and other ground truth data should be performed if the results are to be applied for complex assessments.

References

Aggangan, N., Anarna, J., Cadiz, N., 2019: Tree legume – microbial symbiosis and other soil amendments as rehabilitation strategies in mine tailings in the Philippines. *Philippine Journal of Science.* 14. 481-491.

Alduchov, O., Eskridge, R., 1996: Improved Magnus Form Approximation of Saturation Vapor Pressure. Journal of Applied Meteorology.
doi.org/10.1175/1520-0450(1996)035<0601:imfaos>2.0.co;2

Anjasmara, I.M., Yulyta, S.A., Taufik, M., 2020. Application of time series insar (SBAS) method using sentinel-1a data for land subsidence detection in Surabaya City. International Journal on Advanced Science, Engineering and Information Technology 10, 191–197. doi.org/10.18517/ijaseit.10.1.6749

Brillo, B.B., 2022. Government, premier leader and small lakes' people vis-a-vis lake governance. Social Sciences 11, 165. doi.org/10.3390/socsci11040165

Bzdok, D., Yeo, B.T.T., 2017. Inference in the age of big data: Future perspectives on neuroscience. NeuroImage 155, 549–564. doi.org/10.1016/j.neuroimage.2017.04.061

Carnegie Mellon University, 2014. Smoothing Splines Advanced Methods for Data Analysis (36-402/36-608). URL stat.cmu.edu/~ryantibs/advmethods/notes/smoothspline.pdf (accessed 5.8.25).

Castro, J.M., Moore, J.N., 2000. Pit lakes: Their characteristics and the potential for their remediation. Environmental Geology 39, 1254–1260. doi.org/10.1007/s002549900100

Ge, L., Chang, H.-C., Rizos, C., 2007. Mine subsidence monitoring using multi-source satellite SAR images. Photogrammetric Engineering & Remote Sensing 73, 259–266. doi.org/10.14358/pers.73.3.259

Li, F., Liu, G., Tao, Q., Zhai, M., 2022. Land subsidence prediction model based on its influencing factors and machine learning methods. Natural Hazards 116, 3015–3041. doi.org/10.1007/s11069-022-05796-9

Li, S., Xu, W., Li, Z., 2022. Review of the SBAS insar time-series algorithms, applications, and challenges. Geodesy and Geodynamics 13, 114–126. doi.org/10.1016/j.geog.2021.09.007

Ndahangwapo, N.N., Thiam, D.R., Dinar, A., 2024. Land subsidence impacts and optimal groundwater management in South Africa. Environmental and Resource Economics 87, 1097–1126. doi.org/10.1007/s10640-024-00857-y

Quang, D.N., Linh, N.K., Tam, H.S., Viet, N.T., 2021. Remote sensing applications for reservoir water level monitoring, sustainable water surface management, and environmental risks in Quang Nam Province, Vietnam. Journal of Water and Climate Change 12, 3045–3063. doi.org/10.2166/wcc.2021.347

Raymundo, R., 2017: The Economic Gains from Mining vis a vis Effects on the Environment, Agriculture and Marine Life. Yuchengco Center De La Salle University Manila.

RPN Social, 2022. Baguio: Lubo Lake matatagpuan sa Kibungan, Benguet magiging tourist destinasyon kung malutas ang problema kung sino ang may-ari. Radio Philippine Network News. URL rpnradio.com/baguio-lubo-lake-matatagpuan-sa-kibungan-benguet-magiging-tourist-destinasyon kung-malutas-ang-problema-kung-sino-ang-may-ari/ (accessed 5.8.25)

Samaniego, J., Gibaga, C.R., Tanciongco, A., Rastrullo, R., Mendoza, N., Racadio, C.D., 2020. Comprehensive assessment on the environmental conditions of abandoned and inactive mines in the Philippines. ASEAN Journal on Science and Technology for Development 37. doi.org/10.29037/ajstd.623

Sekkeravani, M.A., Bazrafshan, O., Pourghasemi, H.R., Holisaz, A., 2022. Spatial modeling of land subsidence using machine learning models and statistical methods. Environmental Science and Pollution Research 29, 28866–28883. doi.org/10.1007/s11356-021-18037-6

State of Nevada Department of Conservation & Natural Resources, n.d.. Pit Lakes. Nevada Division of Environmental Protection. Nevada Division of Environmental Protection. URL ndep.nv.gov/uploads/land-mining-faq-docs/Pit_Lakes.pdf (accessed 5.8.25)

Sulapas, J.J., Ybañez, A.A., Marasigan, K.M., Grageda, J.M., Lagmay, A.M., 2024. . Ground subsidence in major Philippine metropolitan cities from 2014 to 2020. doi.org/10.2139/ssrn.4779261

The Cordilleran Sun, 2018. "Lubo Lake in Lubo, Kibungan, Benguet. From a conversation I've had with a local there, the lake is a remnant of an old mining operation. Today, some locals raise tilapia on the lake." - Daniel Feliciano. URL facebook.com/photo.php?fbid=2156445517908785&id=1453599174860093&set=a.1456258857927458 (accessed 5.13.25)

van Dam, T., Wahr, J., Milly, P.C., Shmakin, A.B., Blewitt, G., Lavallée, D., Larson, K.M., 2001. Crustal displacements due to continental water loading. Geophysical Research Letters 28, 651–654. doi.org/10.1029/2000gl012120

Wei, X., Zhao, R., Huang, D., Zhao, Z., 2021. Water evaporation rate correlation based on Dalton model of enclosed space in frost-free refrigerator. Case Studies in Thermal Engineering 28, 101495. doi.org/10.1016/j.csite.2021.101495